Available online at www.sciencedirect.com
SCIENCE DIRECT
Journal of Molecular Catalysis A: Chemical 247 (2006) 206–212
JOURNAL OF MOLECULAR CATALYSIS A: CHEMICAL
www.elsevier.com/locate/molcata

Effect of catalyst pore size on the catalytic performance of silica supported cobalt Fischer–Tropsch catalysts

Dechen Song, Jinlin Li *

Key Laboratory of Catalysis and Materials Science of Hubei Province, College of Chemistry and Materials Science, South-Central University for Nationalities, Wuhan 430074, China

Received 21 September 2005; received in revised form 14 November 2005; accepted 16 November 2005
Available online 4 January 2006

Abstract

A series of cobalt catalysts supported on silica with different pore size were prepared by incipient wetness impregnation method. N_2 physisorption, XRD, H_2-TPR, H_2-TPD, DRIFTS and O_2 pulse reoxidation were used to characterize the catalysts. The results showed that the pore size of the support had a significant influence on the Co_3O_4 crystallite diameter, catalyst reducibility and Fischer–Tropsch activity. The larger pore could cause the Co/SiO_2 to form larger Co_3O_4 crystallite and decreased its dispersion. Catalysts with different pore size showed different CO adsorption property. The catalysts with pore size of 6–10 nm displayed higher Fischer–Tropsch activity and higher C_{5+} selectivity, due to the moderate particle size and moderate CO adsorption on the catalysts.

Keywords: Fischer–Tropsch synthesis; Cobalt; Silica; Pore size; Particle size

1. Introduction

Fischer–Tropsch (FT) synthesis is one of the most promising ways for coal and natural gas conversion to ultra-clean fuels at economically feasible cost [1,2]. Supported cobalt is the preferred catalyst for the Fischer–Tropsch synthesis of long-chain paraffins from natural gas because of its high activity, low water-gas shift activity, and comparatively low cost [3]. Silica is commonly used as the support material due to its high surface area and its inertness. Furthermore, well-dispersed active phases can be obtained [4]. The support's texture and surface acidity, etc. have significant influence on cobalt dispersion, reducibility and catalytic performance.

Bechara et al. [5] found that the support's porosity modified the catalytic properties through their effects on the reducibility of the active phase. Xiong et al. [6] reported that the pore size of alumina support significantly influenced the Co_3O_4 crystallite diameter, catalyst reducibility and FT activity. In the investigated range (10–15 nm), the larger pore size enhanced the formation of bigger Co_3O_4 crystallite, decreased the number of cobalt active sites on the catalyst surface and their reducibility, resulting in a decrease in FT activity.

Ernst et al. [7] studied the FT activity and selectivity of Co/SiO_2 prepared by a sol–gel technique in acid and base media. It was found that the activity for FT increased with the specific surface area, and the selectivity for higher molecular weight hydrocarbon was favored in the case of catalyst with pore diameter of support less than 4 nm. Khodakov et al. [8] investigated the pore size effects on Fischer–Tropsch reaction rates and selectivities over cobalt catalysts using periodic (SBA-15 and MCM-41) and commercial mesoporous silicas as supports. They found that the Fischer–Tropsch reaction rates and C_{5+} selectivities were much higher on cobalt catalysts with the support pore diameter exceeding 3 nm than on the narrower pore catalysts.

From a survey of the literatures, we found that the effect of support and its porosity on FT reaction and hydrocarbon selectivities remained not well understood. This work focused on the effects of pore size on the structure of the Co species and their catalytic behavior in FT synthesis for Co supported on commercial silicas with different pore size. Nitrogen physisorption, X-ray diffraction (XRD), temperature programmed reduction (TPR), diffuse reflectance FTIR spectroscopy (DRIFTS), hydrogen temperature programmed desorption (H_2-TPD) and oxygen

* Corresponding author. Tel.: +86 27 67843016; fax: +86 27 67842752.
E-mail address: lij@scuec.edu.cn (J. Li).

1381-1169/$ – see front matter © 2005 Elsevier B.V. All rights reserved.
doi:10.1016/j.molcata.2005.11.021

Table 1
Pore data of the supports and Co/SiO_2 catalysts

Sample	Surface area (m^2/g)	Average pore diameter (nm)	Volume (cm^3/g)
$SiO_2(1)$	610.5	2.4	0.33
$SiO_2(2)$	457.3	6.8	0.78
$SiO_2(3)$	359.0	10.4	0.93
$SiO_2(4)$	304.5	15.8	1.20
$Co/SiO_2(1)$	524.3	2.2	0.19
$Co/SiO_2(2)$	359.3	6.6	0.59
$Co/SiO_2(3)$	277.8	10.1	0.70
$Co/SiO_2(4)$	233.6	15.7	0.92

pulse reoxidation were used to characterize the catalysts. The activity and selectivity for the FT reaction were investigated in a fixed bed reactor under typical hydrocarbon synthesis conditions (503 K and 10 bar).

2. Experimental

2.1. Catalyst preparation

The SiO_2 supports were obtained from Qingdao Meigao Chemical Co. All the amorphous silicas were characterized using nitrogen physisorption and the results were given in Table 1. The SiO_2 supports with different pore size were designated as $SiO_2(1)$, $SiO_2(2)$, $SiO_2(3)$, $SiO_2(4)$ respectively (see Table 1), were calcined at 773 K for 6 h. The Co/SiO_2 catalysts were prepared by incipient wetness impregnation method. The calcined SiO_2 was impregnated with the appropriate $Co(NO_3)_2{\cdot}6H_2O$ solution, then dried at 383 K for 12 h. Finally, the catalyst precursor was calcined in air at 673 K for 6 h. All the Co/SiO_2 catalysts contain 15 wt.% cobalt (as metal Co) and were denoted as $Co/SiO_2(1)$, $Co/SiO_2(2)$, $Co/SiO_2(3)$, $Co/SiO_2(4)$ correspondingly. Average particle size of catalysts was 40–80 mesh.

2.2. Catalyst characterization

2.2.1. Surface area, pore size distribution and pore volume

Pore size distribution, BET surface area and pore volume were measured by nitrogen physisorption at 77 K using Micromeritics ASAP 2405 instrument. Prior to the measurements, the samples were degassed for 4 h at 373 K in flowing helium (30 ml/min). The pore size distribution and pore volume were determined by the BJH method and the specific surface area was estimated by the BET method.

2.2.2. Temperature programmed reduction (TPR)

The reduction behavior and the interaction between the active phase and the support of each catalyst were examined by using temperature programmed reduction (TPR) technique. TPR experiment was carried out with Zeton Altamira AMI-200 instrument. The catalyst (ca. 0.15 g) was placed in a quartz tubular reactor fitted with a thermocouple for continuous temperature measurement. The reactor was heated with a furnace designed and built to stabilize the temperature gradient and minimize the temperature error. Prior to the TPR measurement, the catalyst was flushed with high purity argon at 423 K for 1 h to drive away water or impurities, and then cooled down to 323 K. Then 10% H_2/Ar was switched on and the flow rate through the reactor was controlled at 30 ml/min. The temperature was raised at a rate of 10 K/min from 323 to 1073 K and was held at the final temperature for 30 min. The H_2 consumption (TCD signal) was recorded automatically by a PC.

2.2.3. Hydrogen temperature programmed desorption (H_2-TPD) and oxygen pulse reoxidation

Hydrogen TPD was carried out in a U-tube quartz reactor with Zeton Altamira AMI-200 device. The sample (ca. 0.15 g) was reduced at 723 K for 12 h using a flow of high purity hydrogen and then cooled under hydrogen stream to 373 K. The sample was held at 373 K for 1 h under flowing argon to remove physisorbed and/or weakly bound species. Subsequently, the sample was slowly increased to 723 K under flowing argon to desorb the remaining chemisorbed hydrogen and the TCD began to record the signal until the signal returned to the baseline. The TPD spectra were integrated and the amount of desorbed hydrogen was determined by comparing to the mean area of calibrated hydrogen pulses.

Oxygen pulse reoxidation was also performed with the Zeton Altamira AMI-200 device. After reduction under the conditions as described above for H_2-TPD, the catalyst was reoxidized at 723 K by injecting pulses of high purity oxygen in argon. All flow rates were set to 30 ml/min. The uncorrected dispersions are based on the assumption of complete reduction of cobalt oxide, and the corrected dispersions are reported by percentage reduction. Without including the percentage of reduction in the calculation, the percentage dispersion is underestimated and, therefore, the resulting crystallite diameter will be overestimated. This correction to the dispersion becomes particularly important in the study of promoted catalysts [9]. The extent of reduction was calculated by assuming metal Co was converted to Co_3O_4.

The calculations of dispersion ($D_{\text{uncorrected}}$) are based on the assumption that the H:Co stoichiometric ratio is 1:1, therefore:

$$D_{\text{uncorrected}}\,(\%) = \frac{N_{\text{surface}}}{N_{\text{total}}} \times 100 = \frac{N_{\text{H}_2} \times 2}{N_{\text{total}}} \times 100$$

Here,

$$N_{\text{H}_2}\,(\text{mol}) = \frac{S_{\text{TPD}}\frac{V_{\text{loop}}}{S_{\text{pulse}}}}{24.5 \times 10^6\ \mu\text{l/mol}}, \qquad D_{\text{corrected}}\,(\%) = \frac{N_{\text{surface}}}{N_{\text{total}}R}$$

where N_{surface} is the mole number of Co^0 on the surface of sample, mol; N_{total} is the total mole number of Co^0 in sample, mol; N_{H_2} is the mole number of H_2 uptake, mol; R is the percentage reduction; D is the catalyst dispersion; S_{TPD} is the analytical area from TPD; V_{loop} is the loop calibration volume, μl; S_{pulse} is the mean area of hydrogen pulses.

Assuming $3Co^0 + 2O_2 = Co_3O_4$, there exists

$$R(\%) = \frac{N_{O_2} \times \frac{3}{2}}{N_{total}} \times 100, \qquad N_{O_2}\,(\text{mol}) = \frac{S_{reoxidation} \frac{V_{loop}}{S_{pulse}}}{24.5 \times 10^6\ \mu\text{l/mol}}$$

where N_{O_2} is the mole number of O_2 uptake; $S_{reoxidation}$ is the area of O_2 pulse reoxidation.

Defining the dispersion in this way, an estimate of the actual crystallite diameter can be determined as follows:

$$d = \frac{6000}{\rho S_{max} D}$$

where d is the diameter of spherical crystallite; S_{max} is the maximum area for pulse; ρ is the density of metal.

2.2.4. X-ray powder diffraction (XRD)

X-ray powder diffraction measurement was performed at room temperature in a Phillips X'pert powder diffractometer with monochromatized Cu Kα radiation. The scan was ranged from 10° to 90° with 0.02° steps. Cobalt phases were detected by comparing the diffraction patterns with those in the standard powder XRD file compiled by the joint committee on powder diffraction standards (JCPDS) published by the International Center for Diffraction Data. Co_3O_4 crystallite diameters were calculated using the Scherrer equation from the most intense Co_3O_4 peak at $2\theta = 36.9°$.

$$d = \frac{0.89\lambda}{B\cos\theta} \times \frac{180^\circ}{\pi}$$

where d is the mean crystallite diameter, λ the X-ray wave length (1.54056 Å), and B is the full width half maximum (FWHM) of the Co_3O_4 diffraction peak.

2.2.5. Diffuse reflectance FTIR spectroscopy (DRIFTS)

The diffuse reflectance FTIR spectra were recorded with a resolution of 2 cm^{-1} and accumulation of 40 on a Nicolet NEXUS 470 FTIR spectrometer supplied with a MCT detector and a diffuse reflectance attachment. The high purity carbon monoxide (>99.99%) was used as probe gas. Argon and hydrogen (>99.999%) were used as the flushing gas and the reducing gas, respectively. The catalyst (30–40 mg) was placed in an infrared cell with ZnSe windows. The catalyst was reduced in situ for 10 h under atmospheric pressure with a stream of hydrogen at 673 K. Subsequently, the system was cooled down to 298 K. After introduction of carbon monoxide for 30 min, the catalyst was purged with argon for 5 min to remove gaseous carbon monoxide before the IR spectra were recorded.

2.3. Fischer–Tropsch synthesis

Fischer–Tropsch synthesis was performed in a fixed bed reactor (i.d. 2 cm) at 503 K and 10 bar. The catalyst (ca. 3.0 g) was mixed with 36.0 g carborundum (200–460 mesh) and 80 g glass bead (diameter of 4–6 mm) to minimize the temperature gradient and reduced in situ with H_2 at atmosphere pressure. The reactor temperature was increased in a H_2 flow of 6 SL h^{-1} g^{-1} from ambient to 373 K, held at 373 K for 60 min, then increased to 723 K in 2 h and held at that temperature for 12 h. Subsequently, the reactor was cooled down to 453 K. The syngas (H_2/CO = 2) was introduced to the reactor and the pressure was increased to 10 bar. The reactor temperature was increased to 503 K in 7 h and the reaction was carried out at 503 K. The wax and water mixture were collected in a hot trap (403 K), and the oil and water were collected from a cold trap (271 K). The effluent product gas was passed through an Agilent 3000 GC for online analysis. The liquid product analysis was performed with an Agilent 6890 GC equipped with a FID detector. The solid wax was dissolved in dimethylbenzene and analyzed with an Agilent 4890 GC. Preliminary experiments in our group showed that steady state has been reached after an initial reaction of 24 h under the reaction condition. The duration sampling was more than 50 h to achieve a good mass balance at the steady state. The carbon monoxide conversion and hydrocarbon selectivity were measured at steady state and have been averaged over the period of constant operation. The carbon monoxide conversion and hydrocarbon selectivity were calculated by these formulas as follows:

$$\text{CO conversion}\,(\%) = \frac{\text{moles of inlet CO} - \text{moles of outlet CO}}{\text{moles of inlet CO}} \times 100$$

$$\text{CH}_4\ \text{selectivity}\,(\%) = S_{CH_4} = \frac{\text{moles of CH}_4\ \text{produced}}{\text{moles of inlet CO} - \text{moles of outlet CO} - \text{moles of CO}_2\ \text{produced}} \times 100$$

$$\text{C}_x\ \text{selectivity}\,(\%, x = 2\text{–}4) = S_{C_x} = \frac{\text{moles of C}_x\ \text{produced}}{\text{moles of inlet CO} - \text{moles of outlet CO} - \text{moles of CO}_2\ \text{produced}} \times 100$$

$$\text{C}_{5+}\ \text{selectivity} = 1 - S_{CH_4} - S_{C_2} - S_{C_3} - S_{C_4}$$

$$\text{CO}_2\ \text{selectivity}\,(\%) = \frac{\text{moles of CO}_2\ \text{produced}}{\text{moles of inlet CO} - \text{moles of outlet CO}} \times 100$$

3. Results and discussion

3.1. Nitrogen physisorption measurements

The BET surface area, pore size and pore volume data of the supports and the Co/SiO_2 catalysts are listed in Table 1. It can be seen that the surface area of support decreased with increasing pore size. Cobalt addition caused the pore diameter of support to decrease slightly, and the pore volume to decrease significantly. Fig. 1 shows that the pore size distributions of all supports were well defined, and the maximum distribution centered at 3, 6, 10 and 15 nm, respectively, consistent with the results of average pore size.

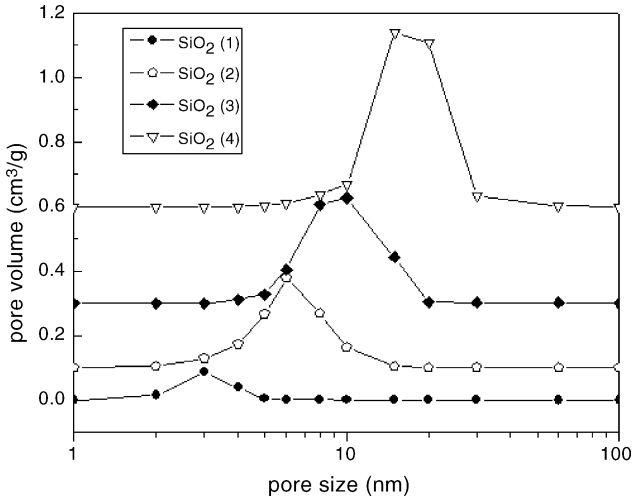

Fig. 1. Pore size distribution of the supports with different pore size.

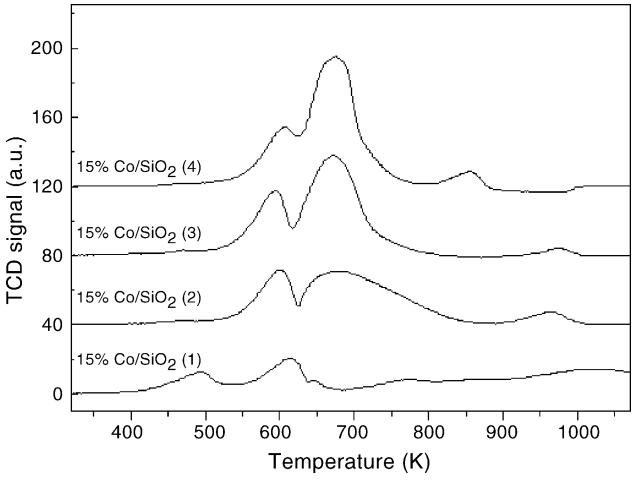

Fig. 2. TPR profiles for calcined catalysts with different pore size.

3.2. Temperature programmed reduction (TPR)

The influence of pore size on the reduction behavior of the Co/SiO_2 catalysts was studied by TPR. Fig. 2 shows the TPR profiles of the Co/SiO_2 catalysts. The occurrence of multiple reduction peaks indicates the presence of a number of reducible cobalt species. Obviously, all the TPR profiles show two major regions: a lower temperature region located between 573 and 723 K and a higher temperature region located between 723 and 1073 K. The TPR peaks in the temperature range of 573–723 K could be assigned to the two step reduction of Co_3O_4 ($Co_3O_4 \rightarrow CoO \rightarrow Co^0$) [10,11]. The broad peak between 723 and 1073 K is related to the reduction of cobalt oxide species (Co^{2+} and Co^{3+}), which interact with the support and difficult to be reduced [12,13]. It can be seen that the low temperature peak changes slightly but the high temperature peak shifts significantly towards lower temperature with increasing pore size of the support, indicating that the interaction of cobalt oxide species with support becomes weaker with increasing pore size. The small peak of $Co/SiO_2(1)$ at around 490 K can be assigned to the reductive decomposition of residual $Co(NO_3)_2$ [14,15]. For $Co/SiO_2(1)$ with small pore size support, the interaction of the cobalt salt and the support was so strong that some cobalt nitrate did not decompose during the calcination of the catalyst precursor. For supports with pore size over 6 nm, the interaction of cobalt salt and support became weaker and all the cobalt nitrate decomposed after calcination.

3.3. H_2-temperature programmed desorption (H_2-TPD) and O_2 pulse reoxidation

Table 2 shows the H_2-TPD and O_2 pulse reoxidation data of the catalysts. It can be seen that the support pore size has remarkably influenced the cobalt dispersion and reducibility. Cobalt crystallite diameter increases with the increase of pore size, consistent with the XRD result. With increasing pore size of the support, the amount of chemisorbed H_2 of reduced catalyst has decreased progressively except the $Co/SiO_2(1)$, suggesting that the number of cobalt active sites on the surface of catalyst decreased. The amount of O_2 uptake first increased and then decreased with increasing pore size of the support, similar to the trend of the reducibility. The catalyst $Co/SiO_2(1)$ with the smallest pore size and largest surface area showed the lowest degree of reduction. On impregnation of the small pore $SiO_2(1)$, there was a drastic ~40% decrease in pore volume (from Table 1) presumably caused by blockage of the smaller pores by the cobalt oxides. These cobalt species were not easily reducible, hence the much lower reducibility of the $Co/SiO_2(1)$. This is consistent with what had previously reported that small particles in narrow pores were more difficult to be reduced than larger particles in wide pores [8]. The Co dispersion decreased with increasing

Table 2
The H_2-TPD and O_2 pulse reoxidation data of Co/SiO_2 catalysts

Sample	H_2 desorbed (μmol/g)	$D_{uncorrected}$ (%)[a]	$Diameter_{uncorrected}$ (nm)[b]	O_2 uptaked (μmol/g)	$D_{corrected}$ (%)[c]	Reducibility (%)	$Diameter_{corrected}$ (nm)[d]
$Co/SiO_2(1)$	42.2	9.6	10.8	292.7	55.9	17.2	1.9
$Co/SiO_2(2)$	115.8	13.6	7.6	879.1	26.5	51.6	3.9
$Co/SiO_2(3)$	94.4	11.1	9.3	812.3	23.4	47.6	4.4
$Co/SiO_2(4)$	64.8	5.1	20.3	655.7	13.2	38.5	7.8

[a] The uncorrected catalyst dispersion.
[b] The uncorrected metal crystallite diameter.
[c] The corrected catalyst dispersion.
[d] The corrected metal crystallite diameter.

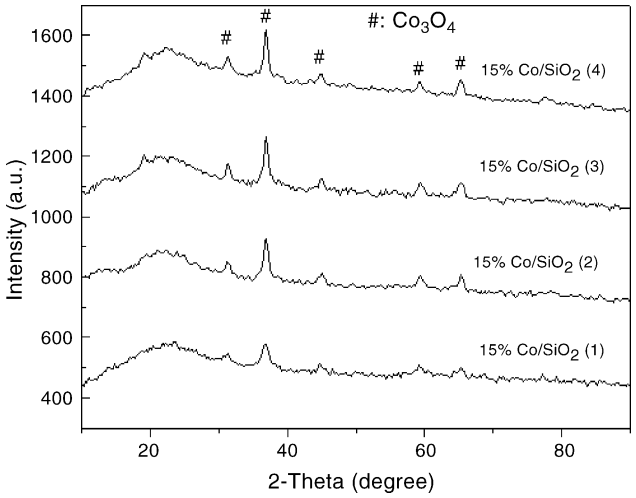

Fig. 3. The XRD patterns of the calcined Co/SiO_2 catalysts.

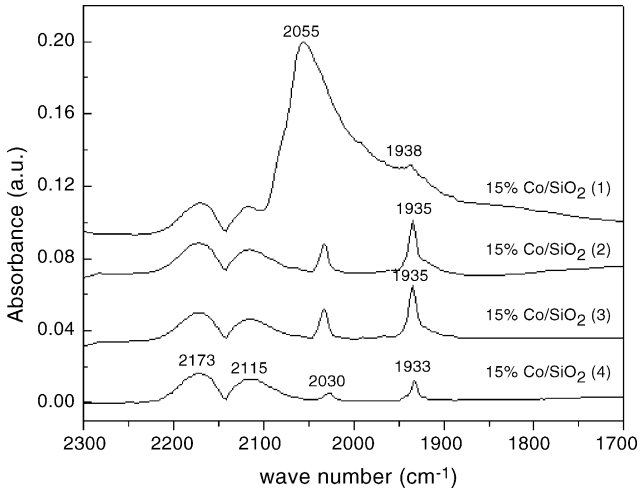

Fig. 4. FTIR spectra of CO adsorbed on Co/SiO_2 catalysts.

pore size of the support, which is also consistent with the results reported by Lapszewicz et al. [16] and Tsubaki et al. [17].

3.4. X-ray powder diffraction (XRD)

X-ray powder diffraction patterns of the catalysts are presented in Fig. 3. For all the catalysts, the cobalt species are present mainly in the form of spinel Co_3O_4. With increasing support pore size the peaks become sharper. Table 3 shows the Co_3O_4 crystallite diameter calculated using the Scherrer equation. It can be seen that the Co_3O_4 crystallite diameter increases with increasing support pore size. Similar results have been reported for cobalt supported on alumina [6].

3.5. DRIFTS

The diffuse reflectance FTIR spectra of adsorbed CO on the Co/SiO_2 catalysts are shown in Fig. 4. A number of changes occurred in the IR spectra with increasing support pore size. For all the catalysts, four peaks were observed. The peaks at 2173 and 2115 cm^{-1} were assigned to gaseous carbon monoxide [18]. The peak at 2030 cm^{-1} was assigned to CO adsorbed on cobalt particles in linear geometry, and the peak at 1935 cm^{-1} was due to the bridged CO adsorbed on cobalt metals [19]. For $Co/SiO_2(1)$ the peak intensity at 2055 cm^{-1} was very big and almost overlapped the peak at 1938 cm^{-1}. It could be attributed to CO linearly adsorbed on Co^0 or Co^+ [20,21]. As the pore size of the support increased, the peak at about 1935 cm^{-1} shifted slightly to lower wave number (1938 → 1935 → 1935 → 1933 cm^{-1}), suggesting that the bridged CO adsorbed on the catalysts became stronger [22,23] with increasing pore size.

Generally large cobalt particle provided large flat metallic surface, favoring bridge-type adsorbed CO, and small particle provided more edges and corners, favoring for CO adsorption in linear geometry [24,25]. For the catalyst $Co/SiO_2(1)$ with small pore size, the well dispersed cobalt with small particle size could provided more edge and corner sites for CO to adsorb linearly. There are similar amount of CO adsorbed in linear-type and bridged-type both on $Co/SiO_2(2)$ and $Co/SiO_2(3)$. However, the peak intensities of bridged CO adsorption at 1935 cm^{-1} on $Co/SiO_2(2)$ and $Co/SiO_2(3)$ were stronger than $Co/SiO_2(4)$, indicating that there were more active sites available in $Co/SiO_2(2)$ and $Co/SiO_2(3)$ than in $Co/SiO_2(4)$, although the cobalt particles in $Co/SiO_2(4)$ was larger than in $Co/SiO_2(2)$ and $Co/SiO_2(3)$. It maybe due to the fact that larger particles of cobalt decreased the number of active sites, resulting in fewer bridged CO adsorption. The results indicated that only cobalt particles with appropriate size could provide the optimum number of active sites, particles that are too small or too big would be unfavorable for CO adsorption.

Table 3
Average Co_3O_4 crystallite diameter for calcined Co/SiO_2 catalysts with different pore size

Sample	Co_3O_4 crystallite diameter (nm)
$Co/SiO_2(1)$	9.0
$Co/SiO_2(2)$	13.0
$Co/SiO_2(3)$	14.3
$Co/SiO_2(4)$	17.0

3.6. Fischer–Tropsch synthesis

The activity and selectivity results for FT synthesis are listed in Table 4. It can be seen that the activity and the selectivity of the catalysts seemed to be very sensitive to the porosity of silica support. The CO conversion first increased and then decreased with increasing catalyst pore size. The C_{5+} selectivity has similar trend to the CO conversion. The catalysts with pore size of 6–10 nm displayed high FT activity and high C_{5+} selectivity.

Many studies of FT synthesis have suggested that the pore size of support could significantly affect the FT reaction rate and hydrocarbon selectivity. Okabe et al. [26] reported that wide pore catalysts are preferable for higher conversion and higher C_{5+} selectivity because of higher reducibility of large cobalt particles in wide pores over the pore size range from 4 to 10 nm. Ohtsuka et al. [27] prepared cobalt catalysts supported by SBA-

Table 4
The performance of different catalysts on Fischer–Tropsch synthesis ($H_2/CO = 2$, $P = 10$ bar, $T = 503$ K, GHSV = 4000 h^{-1})

Catalysts	Pore size (nm)	CO conversion (%)	CO_2 selectivity (%)	Hydrocarbon selectivity (mol%)				
				CH_4	C_2	C_3	C_4	C_{5+}
$Co/SiO_2(1)$	2.2	19.3	2.2	36.4	1.8	1.1	0.9	59.9
$Co/SiO_2(2)$	6.6	65.7	1.1	11.0	0.7	0.6	0.5	87.2
$Co/SiO_2(3)$	10.1	56.5	1.0	11.8	0.9	0.8	0.6	85.9
$Co/SiO_2(4)$	15.7	8.7	1.2	19.3	2.0	0.8	0.7	77.1

15 with different pore diameters using ethanol solution of cobalt acetate. They found that the catalyst with moderate pore diameter of 8.3 nm provided the highest CO conversion. Saib et al. [28] also reported that the catalyst supported by silica with average pore diameter of 10 nm was the most active and selective for hydrocarbon formation in FT synthesis. The C_{5+} and methane selectivity passed through a maximum and a minimum at the 10 nm supported catalyst, respectively.

Support effects on the product selectivity are more complicated than on the activity. Our results also shows that the porosity of support silica affect not only the cobalt particle size but also the product distribution. From Table 4 it can be seen that the C_{5+} selectivity passes through a maximum with increasing pore size and reaches its peak value at $Co/SiO_2(2)$. The CH_4 selectivity has the reverse trend.

Table 4 shows higher methane selectivity for catalyst $Co/SiO_2(1)$ with narrow pore size. As compared with $Co/SiO_2(2)$, the methane selectivity drops from 36.4% to 11.0%. Several reasons have been given to explain the higher methane selectivity in FT synthesis. Zhang et al. [23] and Li et al. [29] explained that the high methane selectivity could be attributed to the sites of weak carbon monoxide adsorption. It is generally assumed that heavier hydrocarbons are favored when carbon monoxide and intermediates are strongly adsorbed by the metal sites [30]. Girardon et al. [31] reported that the unreduced oxide phase could catalyze water-gas shift reaction when cobalt catalysts were not completely reduced and resulted in high yield of carbon dioxide and methane. Our data do not agree with this interpretation, since the content of carbon dioxide was low although the reducibility of $Co/SiO_2(1)$ was poor (from Table 2). Some authors [16,32] considered that the diffusion limitation for carbon monoxide in catalysts pore could increase H_2/CO ratio in catalyst pore and thus increase the methane selectivity.

From the FTIR data, we can see that the peak intensity of linearly adsorbed CO is the highest one while the peak of bridged CO adsorbed on $Co/SiO_2(1)$ is the lowest one in the four catalysts with different pore size. On the other hand, the bond of bridged CO adsorbed on catalyst $Co/SiO_2(1)$ is weaker than other three catalysts. Thus, higher methane selectivity observed on $Co/SiO_2(1)$ with narrow pore size is likely attributed to both the weak carbon monoxide adsorption, due to the presence of unreduced cobalt species and the diffusion limitation for carbon monoxide.

The diffusion limitation for carbon monoxide should become not significant because of the large pore size over $Co/SiO_2(4)$ catalyst. The reducibility of $Co/SiO_2(4)$ catalyst was not very low as compared with $Co/SiO_2(2)$ and $Co/SiO_2(3)$ from H_2-TPD. However, the cobalt crystallite diameter in $Co/SiO_2(4)$ was too big, so that the number of cobalt active sites on the surface of Co/SiO_2 catalyst decreased, resulted in a decrease of FT activity. On the other hand, the bond of bridged CO adsorbed on catalyst $Co/SiO_2(4)$ is the strongest among the four catalysts (from FTIR spectra), this may be responsible for the low CO conversion.

The FT synthesis is a complex reaction. There are many factors influencing the reaction rate and hydrocarbon product selectivity. The activity will decrease if the particle sizes of active metal are too small or too big. From our results, we can see that the catalysts with pore size of 6–10 nm exhibited the best performance for FT synthesis, probably due to the moderate particle size and the moderate carbon monoxide adsorption on catalysts.

4. Conclusions

Catalytic and characterization results show that the support porosity influenced strongly the structure, the reducibility, and the FT catalytic performance of silica supported cobalt catalysts. The larger pore size could cause the Co/SiO_2 to form larger Co_3O_4 crystallite. The dispersion of catalysts decreased with increasing pore size. Small pores lead to smaller Co crystallites and to the lower reducibility. With increasing pore size of the support, the interaction of the cobalt oxide species with support became weaker. Catalysts with different pore size showed different CO adsorption property. Only cobalt particles with appropriate size could provide the optimum number of active sites, favoring bridge-type CO adsorption. The catalysts with pore size of 6–10 nm displayed higher FT activity and higher C_{5+} selectivity.

Acknowledgements

The authors gratefully acknowledge the supports from the National Natural Science Foundation of China (20473114, 20590360), Talented Young Scientist Foundation of Hubei (2003ABB013), Excellent Young Teachers Program of the Ministry of Education of China, the State Ethnic Affairs Commission, PR China and Returnee Startup Scientific Research Foundation of the Ministry of Education of China. The authors also thank Prof. Kongyong Liew for helpful discussions in the preparation of this manuscript.

References

[1] H. Schulz, Appl. Catal. A: Gen. 186 (1999) 3.
[2] R.B. Anderson, Fischer–Tropsch Synthesis, Academic Press, New York, 1984.
[3] M.E. Dry, Catal. Today 71 (2002) 227.
[4] M. Glinski, J. Kijenski, A. Jakubowski, Appl. Catal. A: Gen. 128 (1995) 209.
[5] R. Bechara, D. Balloy, D. Vanhove, Appl. Catal. A: Gen. 207 (2001) 343.
[6] H.F. Xiong, Y.H. Zhang, S.G. Wang, J.L. Li, Catal. Commun. 6 (2005) 512.
[7] B. Ernst, S. Libs, P. Chaumette, A. Kiennemann, Appl. Catal. A: Gen. 186 (1999) 145.
[8] A.Y. Khodakov, A.G. Constant, R. Bechara, V.L. Zholobenko, J. Catal. 206 (2002) 239.
[9] G. Jacobs, T. Das, Y.Q. Zhang, J.L. Li, G. Racoillet, B.H. Davis, Appl. Catal. A: Gen. 233 (2002) 263.
[10] W.J. Wang, Y.W. Chen, Appl. Catal. A: Gen. 77 (1991) 228.
[11] J.L. Li, N.J. Coville, Appl. Catal. A: Gen. 208 (2001) 177.
[12] G.R. Moradi, M.M. Basir, A. Taed, Kiennemann, Catal. Commun. 4 (2003) 27.
[13] S. Ribet, D. Tichit, B. Coq, B. Ducourant, F. Morato, J. Solid State Chem. 142 (1999) 383.
[14] E.L. Rodrigues, J.M.C. Bueno, Appl. Catal. A: Gen. 232 (2002) 147.
[15] E. van Steen, G.S. Sewell, R.A. Makhothe, C. Micklethwaite, H. Manstein, M. de Lange, C.T. O'Connor, J. Catal. 162 (1996) 220.
[16] J.A. Lapszewicz, H.J. Loch, J.R. Chipperfield, J. Chem. Soc., Chem. Commun. (1993) 819.
[17] N. Tsubaki, Y. Zhang, S.L. Sun, H. Mori, Y. Yoneyama, X.H. Li, K. Fujimoto, Catal. Commun. 2 (2001) 311.
[18] J.L. Li, N.J. Coville, Appl. Catal. A: Gen. 181 (1999) 201.
[19] L.E.S. Rygh, C.J. Nielsen, J. Catal. 194 (2000) 401.
[20] A.A. Khassin, T.M. Yurieva, V.V. Kaichev, V.I. Bukhtiyarov, A.A. Budneva, E.A. Paukshtis, V.N. Parmon, J. Mol. Catal. A: Chem. 175 (2001) 189.
[21] M. Jiang, N. Koizumi, T. Ozaki, M. Yamada, Appl. Catal. A: Gen. 209 (2001) 59.
[22] G.Z. Bian, A. Oonuki, Y. Kobayashi, N. Koizumi, M. Yamada, Appl. Catal. A: Gen. 219 (2001) 13.
[23] J.L. Zhang, J.G. Chen, J. Ren, Y.H. Sun, Appl. Catal. A: Gen. 243 (2003) 121.
[24] P. Concepción, C. López, A. Martínez, V.F. Puntes, J. Catal. 228 (2004) 321.
[25] X.Q. Qiu, N. Tsubaki, K. Fujimoto, J. Chem. Eng. Jpn. 34 (11) (2001) 1366.
[26] K. Okabe, X.H. Li, M.D. Wei, H. Arakawa, Catal. Today 89 (2004) 431.
[27] Y. Ohtsuka, Y. Takahashi, M. Noguchi, T. Arai, S. Takasaki, N. Tsubouchi, Y. Wang, Catal. Today 89 (2004) 419.
[28] A.M. Saib, M. Claeys, E.V. Steen, Catal. Today 71 (2002) 395.
[29] Q. Li, X.P. Dai, J.P. Xu, C.C. Yu, S.K. Shen, Chin. J. Catal. 22 (5) (2001) 469.
[30] J.V. Loosdrecht, A.J.V. Dillen, J.W. Geus, Appl. Catal. A: Gen. 150 (1997) 365.
[31] J.S. Girardon, A.S. Lermontov, L. Gengembre, P.A. Chernavskii, A.G. Constant, A.Y. Khodakov, J. Catal. 230 (2005) 339.
[32] M. Kraum, M. Baerns, Appl. Catal. A: Gen. 186 (1999) 189.